2002

Chandra Observation of Supernova Remnant G54.1+0.3: A Close Cousin of the Crab Nebula

FJ Lu

QD Wang
University of Massachusetts - Amherst

B Aschenbach

P Durouchoux

LM Song

Chandra Observation of SNR G54.1+0.3 — a Close Cousin of the Crab Nebula

F.J. Lu[1,2], Q.D. Wang[1], B. Aschenbach[3], Ph. Durouchoux[4], and L.M. Song[2]

ABSTRACT

We present a *Chandra* ACIS observation of SNR G54.1+0.3. This supernova remnant is resolved into several distinct X-ray emitting components: a central bright point-like source (CXOU J193030.13+185214.1), a surrounding ring, bipolar elongations, plus low surface brightness diffuse emission. The spectra of these components are all well described by power-law models; the spectral index steepens with increasing distance from the point-like source. We find no evidence for any thermal plasma emission that would correspond to shocked interstellar medium or ejecta. The observed morphological and spectral characteristics suggest that G54.1+0.3 is the closest "cousin" of the Crab Nebula — a pulsar wind nebula driven by a combination of equatorial and polar outflows from the putative pulsar represented by the point-like X-ray source.

Subject headings: ISM: individual (G54.1+0.3)—ISM: jets and outflows —stars:neutron—supernova remnants—X-rays: ISM

1. Introduction

The Crab Nebula has played an essential role in our understanding of pulsar wind nebulae (PWNe). The basic observational X-ray characteristics of the Crab Nebula are a

---

[1]Astronomy Department, University of Massachusetts, Amherst, MA 01003; lufj@flamingo.astro.umass.edu; wqd@gcs.astro.umass.edu

[2]Laboratory of Cosmic Ray and High Energy Astrophysics, Institute of High Energy Physics, CAS, Beijing 100039, P.R. China; songlm@astrosv1.ihep.ac.cn

[3]Max-Planck-Institut für Extraterrestrische Physik, Postfach 1312, 85741 Garching, Germany; bra@mpe.mpg.de

[4]CE-Saclay, DSM, DAPNIA, Service d'Astrophysique, Gif-sur-Yvette Cedex, France; durvla@discovery.saclay.cea.fr

central pulsar, an ellipse-shaped torus, two jets and the absence of an outer thermal shell. The X-ray torus is explained as shocked equatorial wind material from the central pulsar (e.g., Aschenbach & Brinkmann 1975; Pelling et al. 1987; Weisskopf et al. 2000), while the jets correspond to the outflows from the two rotation poles of the pulsar (e.g., Aschenbach 1992). The observations and modeling of these characteristics have advanced our understanding of the energetics and geometry of pulsar wind, as well as the physics of ultra-relativistic shocks and particle acceleration (e.g., Rees & Gunn 1974; Aschenbach & Brinkmann 1975; Kennel & Coroniti 1984a, 1984b).

However, morphologically the Crab Nebula is unique. No other source has to date been found to mimic all the basic X-ray characteristics of the Crab Nebula (Gaensler 2001). The PWNe surrounding the Vela Pulsar and PSR B1509-58 have X-ray arcs, yet these X-ray arcs are not complete X-ray rings as observed in the Crab Nebula, and furthermore, these two PWNe are embedded inside bright thermal diffuse emission (Helfand, Gotthelf, & Halpern 2001; Gaensler et al. 2001).

In order to deepen our understanding of the properties of the pulsar wind and its interaction with the environments, it is important to find a PWN which closely resembles the Crab Nebula. Supernova remnant (SNR) G54.1+0.3 is such a candidate. Radio emission from G54.1+0.3 is centrally-filled, shows strong polarization, and has a flat spectrum, typical for a Crab-like SNR (Reich et al. 1985; Velusamy & Becker 1988). A nonthermal X-ray spectrum from *ASCA* observations confirmed its Crab-like nature (Lu, Aschenbach, & Song 2001). As we will present in this letter, our recent *Chandra X-ray Observatory* observation of this remnant shows that it is the closest "cousin" of the Crab Nebula.

2.   Observation and Data Reduction

SNR G54.1+0.3 was observed with *Chandra* on 6-7 June 2001. The remnant was positioned at the aimpoint on the back-illuminated CCD chip S3 of the Advanced CCD Imaging Spectrometer (ACIS) in "faint" mode and at a working temperature of -120° C. The spatial resolution is $\sim0\farcs5$, and the spectral resolution is ~120 eV at 2.0 keV. The CCD frame read-out time for this observation is 3.2 seconds.

We calibrated the data using *CIAO* (2.1.3). After excluding two time intervals of high background we obtained a net exposure of 30.9 ks. Based on a comparison of the positions of the X-ray point source CXOU J193034.62+185110.8 (southeast of the remnant, see Fig. 1) and its optical counterpart, we find that the absolute positional accuracy of the X-ray observations is about $0\farcs6$, consistent with the position accuracy claimed in the *Chandra*

Proposer's Observatory Guide.

3. Analysis and Results

While Fig. 1 presents an overview of the *Chandra* data, Fig. 2 is a close-up of G54.1+0.3, with the image data adaptively smoothed using a Gaussian to achieve a signal-to-noise ratio of $\gtrsim 5$. The structure of the remnant is a complex, but we decompose it into several components (Fig. 1): a central bright point-like source (CXOU J193030.13+185214.1), a surrounding ring, elongations to the east and west, and extended low surface brightness emission in between and beyond the central structures. We find no evidence for a shell-like structure that would correspond to the thermal emission usually expected for an SNR. Therefore the remnant resembles the Crab Nebula in morphology quite closely.

Fig. 3 displays spectral model fits of the individual components of G54.1+0.3 and Table 1 lists the corresponding model parameters. The background used in the spectral analysis is extracted from an annulus centered on CXOU J193030.13+185214.1 and with the inner and outer radii equal to $70''$ and $130''$ (with CXOU J193034.62+185110.8 removed). The spectrum of each of these components can be well fitted with a power-law model. There is no evidence for any emission line, and fitting the spectra with thermal models yields temperatures around 10 keV, which is much higher than the plasma temperature ($\lesssim 3$ keV) typically observed for young SNRs. Therefore we detect no significant thermal emission. We assume that the X-ray absorption column density is the same across the field as the absorption column densities of all these components derived from individual spectral fitting are similar. The jointly fitted value ($1.6 \pm 0.1 \times 10^{22}$ cm^{-2}) is about half of the total Galactic X-ray absorption ($\sim 3.6 \times 10^{22}$ cm^{-2}) derived from the *IRAS* 100 μm emission in this direction (Boulanger & Perault 1988; Wheelock et al. 1994). Assuming that the absorbing gas is relatively uniformly distributed along the line of sight, the distance to G54.1+0.3 should be approximately 5 kpc, about half way to the edge of the Galaxy from the Sun.

The source CXOU J193030.13+185214.1 most likely represents the pulsar that powers G54.1+0.3. The radial surface brightness profile of this source is consistent with the point spread function of the instrument. The slow CCD frame read-out time (3.2 s) of the observation, however, prevents a search for any periodicity typical of a young pulsar. We find no significant signal with a period >6 s. The count-rate of the source, 0.064 ± 0.002 cts s^{-1}, indicates a pile-up fraction of only $\sim 6\%$ with a negligible effect on the spectrum. The relation between the photon spectral indices of the source and the nebula is well consistent with the one derived by Gotthelf & Olbert (2001) for pulsars and their respective nebulae. We find no emission peaks at the source position at radio (with 4.8 GHz *VLA* data, Velusamy

& Becker 1988) and infrared (with the online *2MASS* data) wavelengths. From our 0.1-2.4 keV X-ray luminosity (1.8×10^{33} d_5^2 erg s^{-1}, where d_5 is the distance in units of 5 kpc) of this point source, we infer the pulsar spin-down luminosity $\dot{E}$ as $\sim2\times10^{36}$ d_5^2 erg s^{-1} (Becker & Trümper 1997).

An eyeball fit to the ring with an ellipse centered on CXOU J193030.13+185214.1 gives the north-south semi-major axis as 5$\farcs$7 and the east-west semi-minor axis as 3$\farcs$7. The eastern part of the ellipse is much brighter than the western part. The spectrum of the ring is the hardest among the diffuse components.

The two elongations are not as well defined as the ring (Figs. 1-2). The western elongation is oriented perpendicular to the ring and extends $\sim32''$ horizontally from near the central point source to (RA, Dec; J2000) $19^h30^m28^s$, $18°52'14''$. The eastern elongation extends $\sim14''$ ending at about $19^h30^m31^s$, $18°52'10''$. The orientation has an average inclination of $\sim18°$ to the south.

The outer low surface brightness diffuse emission marks the accumulated pulsar wind material. The size of this low surface brightness emission ($1\farcm5 \times 1\farcm2$) is much larger than that of the central bright region ($0\farcm7 \times 0\farcm3$) composed of the point-like source, the ring and the elongations. The low surface brightness component shows some extensions to the west, north and northeast and compares well with the radio map both in size and overall shape (Velusamy & Becker 1988). The spectrum is significantly softer than those of the ring and western elongation, suggesting that, if we assume synchrotron radiation, the particles in this region are more evolved. A detailed comparison and explanation of the X-ray and radio maps and a more extensive study of the low surface brightness diffuse emission will be presented in a separate paper.

4.   Comparison with the Crab Nebula

The X-ray morphology of G54.1+0.3 is strikingly similar to that of the Crab Nebula although some differences exist. Both remnants show a complete X-ray ring (torus) around the corresponding pulsar, plus two opposite elongations (jets), as well as the lack of a thermal outer shell. But the elongations of G54.1+0.3 are more diffuse than the Crab jets, that we will discuss more specifically in §5.2. G54.1+0.3 shows large scale low surface brightness X-ray emission beyond the ring and the elongations. This emission coincides well with the radio morphology of the remnant (Velusamy & Becker 1988). In contrast, little X-ray emission is presented beyond the Crab torus (Weisskopf et al. 2000). The radio size of the Crab Nebula is ~3 times bigger than the X-ray size (Bietenholz & Kronberg 1990; Weisskopf et al. 2000).

The morphological difference of the outer low surface brightness emission suggests that the synchrotron cooling efficiency in the G54.1+0.3 ring is much lower than in the Crab torus.

G54.1+0.3 and the Crab Nebula have quite similar spectral characteristics. The spectra of both remnants are characterized by power-laws which steepen progressively from pulsar, through torus (ring) and jets (elongations), to the outer diffuse emission (Table 1; Willingale et al. 2001). The similar spectral steepening trend indicates that particles follow similar tracks in the two remnants. However, the spectra of G54.1+0.3 are flatter than those of the corresponding components in the Crab Nebula, consistent with lower efficiency of the synchrotron cooling in G54.1+0.3.

Both the total X-ray luminosity and the luminosities of the corresponding components in G54.1+0.3 differ substantially from those of the Crab Nebula (see Table 1 and Weisskopf et al. 2000). The putative pulsar and the X-ray nebula of G54.1+0.3 are about two orders of magnitude less luminous than those of the Crab. The ring of G54.1+0.3 accounts for only about 10% of the total extended emission, but the torus of the Crab Nebula dominates the X-ray emission of the whole nebula. In G54.1+0.3, the luminosities of the elongations are comparable with that of the ring, whereas in the Crab Nebula, the jets are obviously much weaker than the torus. These differences are likely due to the particular pulsar wind geometry and energy input to the various components in the two remnants.

5. Pulsar Wind Properties

We suggest that the X-ray ring and elongations are due to the equatorial wind and the two polar outflows from the pulsar, respectively, as illustrated schematically in Fig. 4.

5.1. The X-ray Ring

The elliptical ring in G54.1+0.3 is apparently the projection of an inclined circular ring. Similar to the X-ray torus in the Crab Nebula, this ring might be due to the shocked pulsar equatorial wind (Aschenbach & Brinkmann 1987). The ratio of observed semi-major and semi-minor axes suggests an inclination angle $\theta=41°$.

Following Pelling et al. (1987), we calculate whether the Doppler boosting of the downstream motion can explain the X-ray brightness variation across the ring (Fig. 5). The intensity (I) of the ring at position angle ϕ measured counter-clockwise from the north can

be expressed as

$$I = I_0 * [\frac{\sqrt{1-v^2}}{1 - \cos(\theta) * v * \sin(\phi)}]^{\alpha+1} + I_b, \tag{1}$$

where I_0 is the unshifted intensity, v is the bulk motion velocity in units of c — the speed of light, α is the photon spectral index, and I_b is the intensity of the diffuse background emission. Fig. 5 shows that the Doppler boosting model fits the measured intensity variation well. The fitted parameters and their 1σ uncertainties are: I_0=7.6±2.4 cts arcsec^{-2}, v=0.40±0.12 c, and I_b=5.7±2.5 cts arcsec^{-2}. Using the v value and following Kennel & Coroniti (1984b) we infer a ratio of the electromagnetic energy flux to the particle energy flux in the wind of $\sigma \simeq 0.06$. Therefore, the surface brightness variation across the ring is consistent with the assumption that the enhanced X-ray emission arises from the freshly shocked pulsar wind material.

5.2. The Elongations

We propose that the elongations are associated with the pulsar polar outflows. This association is suggested by the morphology of the western elongation (Figs. 1-2). The spectrum of the elongation is flatter than that of the surrounding low surface brightness emission, suggesting that the particles in the western elongation have undergone fewer synchrotron losses. The eastern elongation is not well resolved, but appears bent and shorter than the western elongation. These two elongations, however, are broader and more irregular than the relatively well confined jets observed in Crab (Weisskopf et al. 2000), Vela (Helfand et al. 2001), and PSR B1509-58 (Gaensler et al. 2001), indicating that the pulsar polar flows in G54.1+0.3 are less collimated.

5.3. Geometry

The X-ray morphology of the ring and the two elongations in G54.1+0.3 suggest that the pulsar wind is concentrated in the equatorial plane and the polar outflow directions. The width of the ring is about 2″.5 in the minor axis direction. As the radius of the deprojected ring is 5″.7, the width indicates that the equatorial wind particles fan out in a half opening angle of $\lesssim$16°, corresponding to $\lesssim$1.1π steradian. The width of the head of the western elongation is measured to 6″, implying that the half opening angle of the western polar outflow is ∼4°, assuming that the outflow is perpendicular to the equatorial plane as implied by Fig. 2. The corresponding solid angle is 5×10$^{-3}\pi$ steradian. The open angle of the eastern outflow remains unclear because of the insufficient knowledge about its direction

and thus length.

The observed pulsar wind geometry reflects the fractional wind power injected to the ring and elongations. Because the reverse shock occurs when the wind ram pressure balances the diffuse nebula pressure, p_n, we have

$$r_s = \left(\frac{\delta \dot{E}}{\Omega c p_n}\right)^{1/2},\tag{2}$$

where r_s is the distance from the pulsar, δ is the fraction of the wind power $\dot{E}$ in one particular wind component, and Ω is the solid open angle of that component. We assume that $\dot{E}$ is split between $\dot{E}_e$ (injected to the equatorial ring) and $\dot{E}_p$ (released in the polar outflows) that is equally divided between the two polar outflows. We also assume that p_n does not change substantially with position in the diffuse nebula, because the sound speed in a relativistic plasma is $c/\sqrt{3}$ and so no pressure gradient in the bubble can be maintained on time scales that are dynamically important (e.g., Rees & Gunn 1974). From Equation (2), with the geometric parameters and assumptions, we infer that $\gtrsim 1/3$ of $\dot{E}$ is released to the polar outflows.

6. Summary and Conclusions

Based on a *Chandra* ACIS-S observation, we have resolved the spatial and spectral structures of SNR G54.1+0.3. We find that both its morphology and the spectra closely resemble those of the Crab Nebula, though the synchrotron cooling efficiency in G54.1+0.3 may be substantially lower than in the Crab Nebula. In particular, we have discovered a point-like source, CXOU J193030.13+185214.1, at a location close to the morphological center of G54.1+0.3. The source is most likely the pulsar powering the SNR, although a spin period of the pulsar is yet to be determined. We estimate the pulsar spin-down luminosity to be $\sim 2\times 10^{36}\ d_5^2$ erg s^{-1} from the X-ray luminosity of the point source. We suggest that the diffuse X-ray emission around the pulsar originates from the shocked pulsar wind. The presence of the X-ray ring indicates a strong equatorial wind with an inclination angle of 41°. From the surface brightness variation across the ring we infer the downstream flow speed of the shocked pulsar wind material to be 0.40±0.12 c, which indicates that the wind is particle dominated. The two elongations are oriented nearly perpendicular to the ring and are likely to be associated with the polar outflows from the pulsar. The geometry of the X-ray ring and the elongations suggest at least one-third of the spin-down energy is injected into the two polar outflows. These characteristics of SNR G54.1+0.3 provide new constraints for modeling of the elusive pulsar wind and its interaction with the environment.

REFERENCES

Aschenbach, B. 1992, Zeiss Info. Jenaer Rundschau, 1, 6

Aschenbach, B., & Brinkmann, W. 1975, A&A, 41, 147

Becker, W., & Trümper, J. 1997, A&A, 326, 682

Bietenholz, M.F., & Kronberg, P.P. 1990, ApJ, 357, L13

Boulanger, F., & Perault, M. 1988, ApJ, 330, 964

Gaensler, B.M. 2001, in AIP Conf. Proc. 565, Young Supernova Remnants, ed. S.S. Holt & U. Hwang (New York:AIP), 295

Gaensler, B.M., Arons, J., Kaspi, V.M., Pivovaroff, M.J., Kawai, N., & Tamura, K. 2001, ApJ, accepted (astro-ph/0110454)

Gotthelf, E.V., & Olbert, C.M. 2001, astro-ph/0112017

Helfand, D.J., Gotthelf, E.V., & Halpern, J.P. 2001, ApJ, 556, 380

Lu, F.J., Aschenbach, B., & Song, L.M. 2001, A&A, 370, 570

Kennel, C.F., & Coroniti, F.V. 1984a, ApJ, 283, 694

Kennel, C.F., & Coroniti, F.V. 1984b, ApJ, 283, 710

Pelling, R.M., Paciesas, W.S., Peterson, L.E., Makishima, K., Oda, M., Ogawara, W., & Miyamoto, S. 1987, ApJ, 319, 416

Rees, M.J., & Gunn, J.E. 1974, MNRAS, 167, 1

Reich, W., Fürst, E., Altenhoff, W.J., Reich, P., & Junkes, N. 1985, A&A, 151, L10

Velusamy, T., & Becker, R.H. 1988, AJ, 95, 1162

Weisskopf, M.C., et al. 2000, ApJ, 536, L81

Wheelock, S.L., et al. 1994, IRAS Sky Survey Atlas Explanatory Supplement (JPL, Pasadena), JPL Publication 94-11

Willingale, R., Aschenbach, B., Griffiths, R.G., Sembay, S., Warwick, R.S., Becker, W., Abbey, A.F., & Bonnet-Bidaud, J.-M. 2001, A&A, 365, L212

Table 1.   Spectral properties of various components of G54.1+0.3[a]

Components	Photon Index	F_1 [b]	F_2 [b]
Pulsar	$1.09^{+0.08}_{-0.09}$	1.72	2.31
Ring	$1.64^{+0.18}_{-0.16}$	0.52	0.97
Western Elongation	$1.66^{+0.16}_{-0.14}$	0.68	1.30
Eastern Elongation	$1.95^{+0.28}_{-0.26}$	0.20	0.49
Outer Region	$1.97^{+0.11}_{-0.12}$	2.31	6.36

[a]Parameters are from fit with χ^2=366.4 and 386 degree of freedom. The jointly-fitted X-ray-absorbing column density is $1.6\pm0.1\times10^{22}$ cm^{-2}.

[b]F_1 and F_2 are absorbed and unabsorbed fluxes, respectively; both in the 0.2-10.0 keV band and in units of 10^{-12} ergs cm^{-2} s^{-1}.
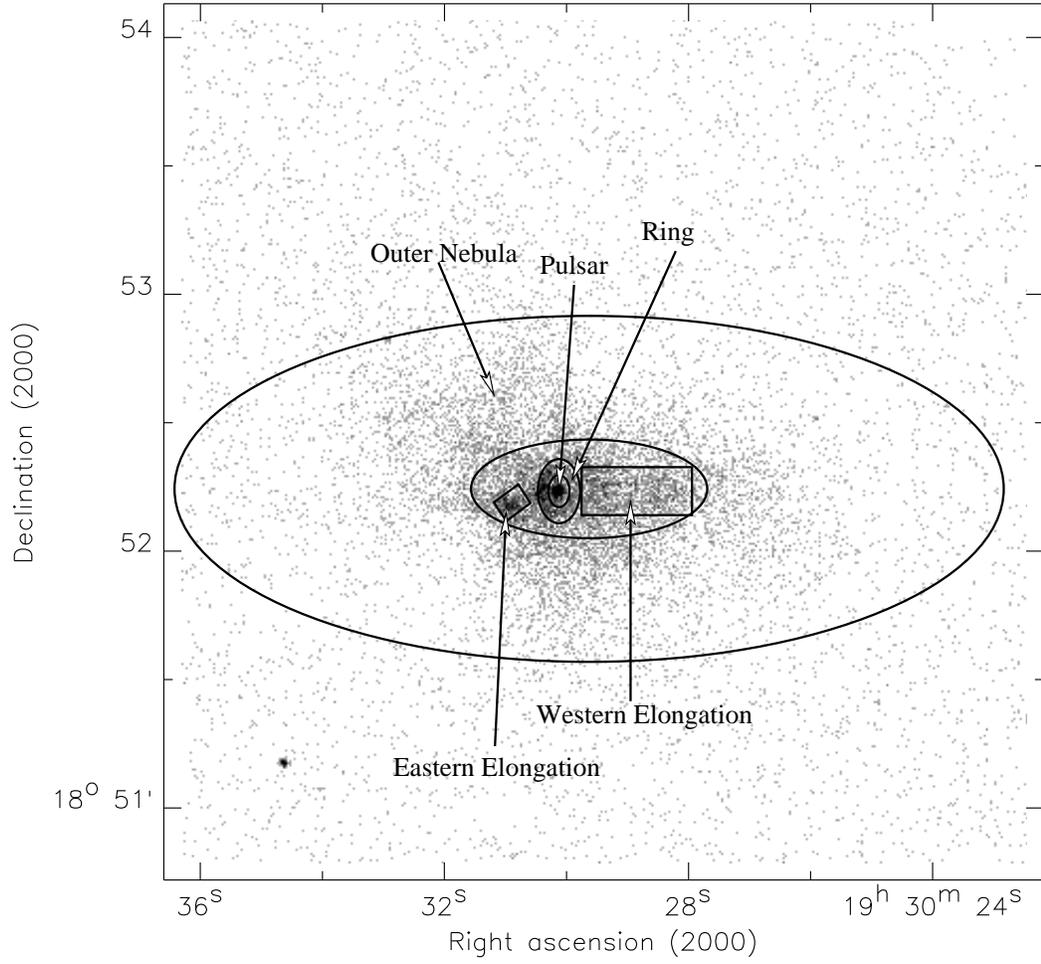
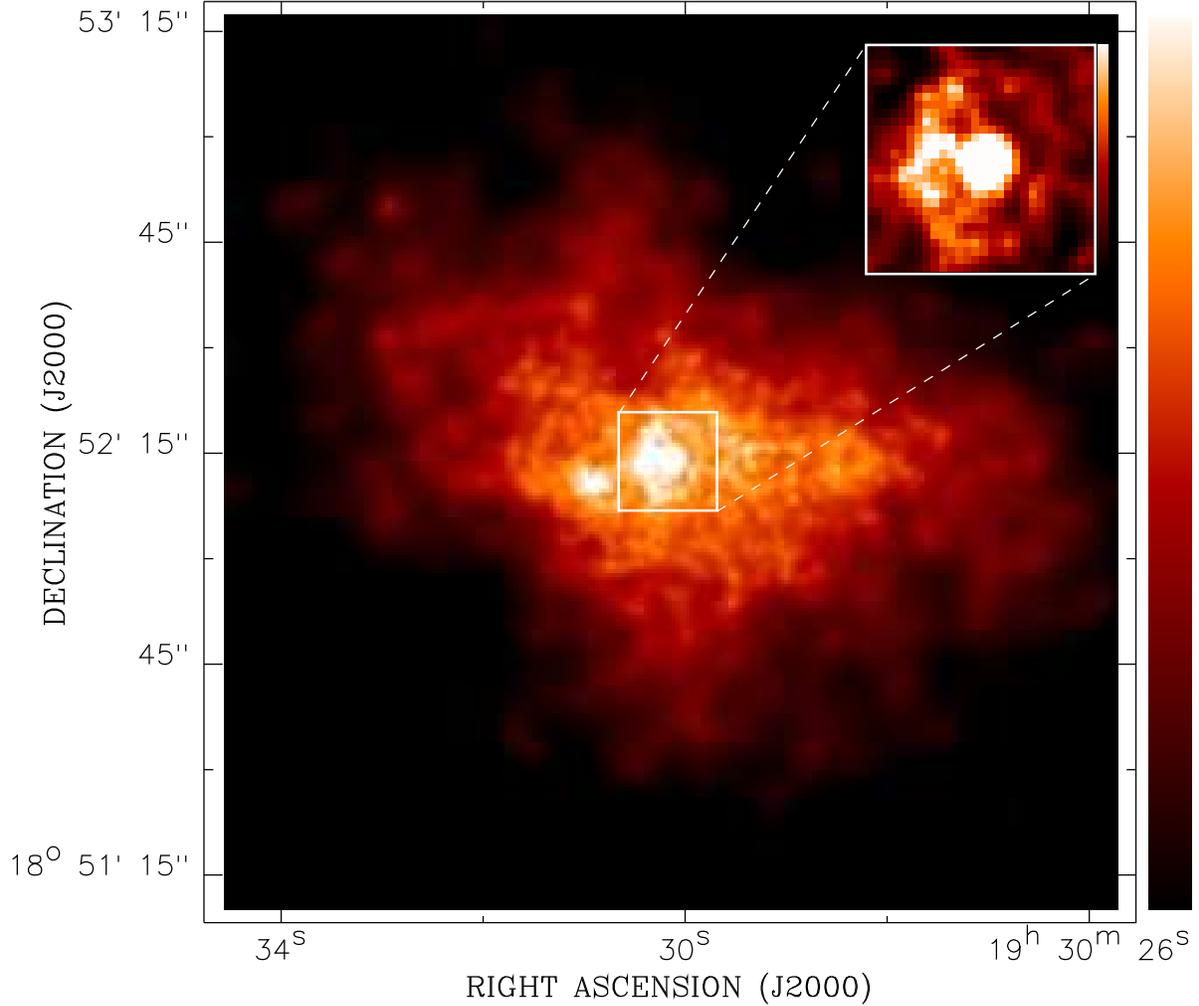Fig. 1.— *Chandra* ACIS-S count distribution in the field of SNR G54.1+0.3. The overlaid

Fig. 2.— *Chandra* ACIS-S X-ray (0.5-10 keV) intensity map of SNR G54.1+0.3. The image is smoothed adaptively with a Gaussian adjusted to achieve signal-to-noise ratio $\gtrsim 5$. The intensity is plotted on logarithmic scale from 7.43×10^{-5} to 5.95×10^{-3} cts cm^{-2} s^{-1} arcmin^{-2}. Shown in the upper-right corner is the central region of SNR G54.1+0.3 plotted on logarithmic scale from 1.49×10^{-3} to 8.92×10^{-3} cts cm^{-2} s^{-1} arcmin^{-2}.
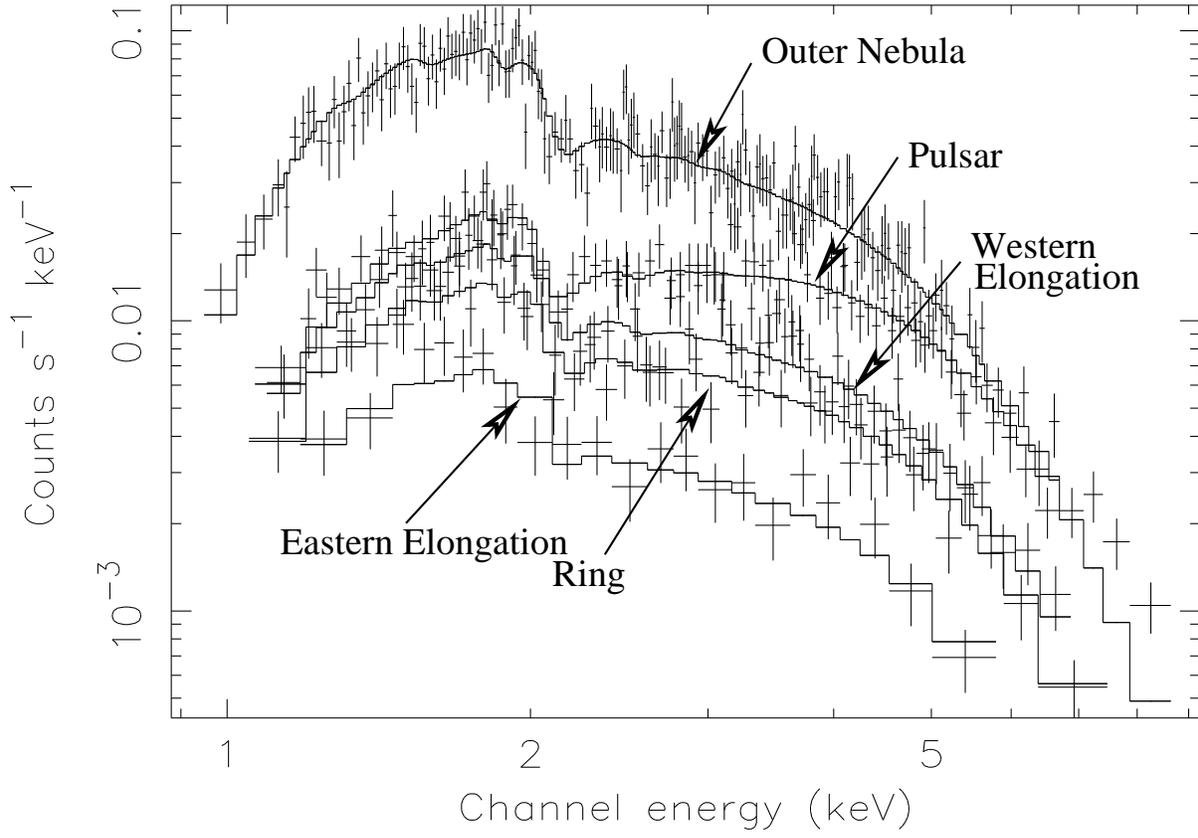
Fig. 3.— Power-law model fits to the spectra of various components of SNR G54.1+0.3.
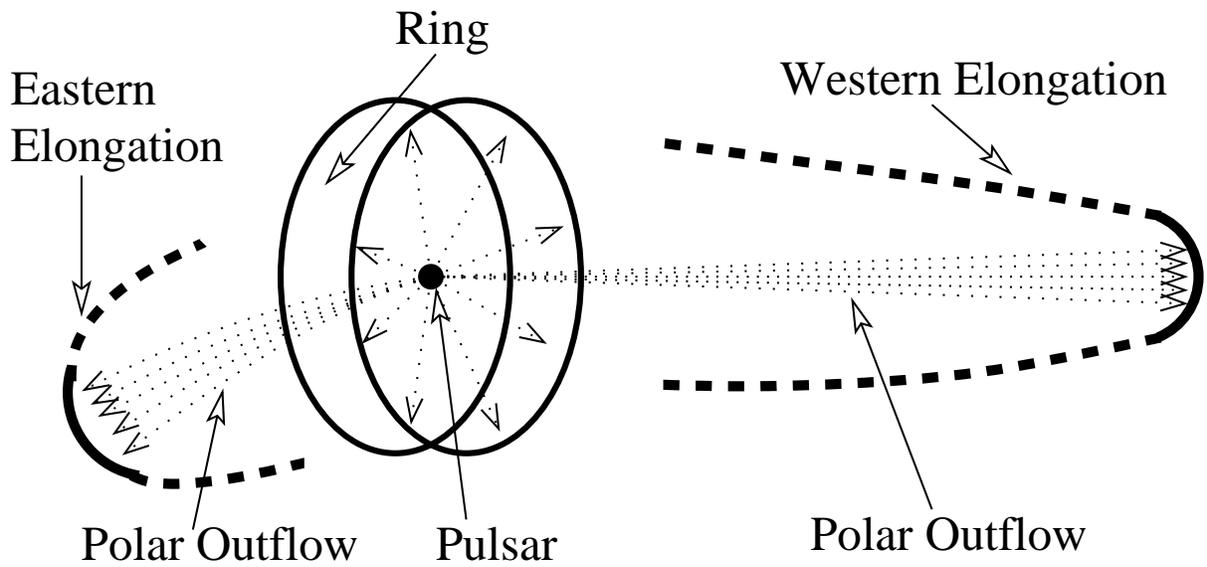
Fig. 4.— Illustration of various components in the central region of SNR G54.1+0.3. The wind from the central pulsar (dotted thin lines) consists of two primary components: an equatorial wind and two polar outflows. The solid lines represent the terminal shocks and the dashed thick lines mark the regions where instabilities and/or bulk material drifted from the terminal shock giving rise to some bright emission features.
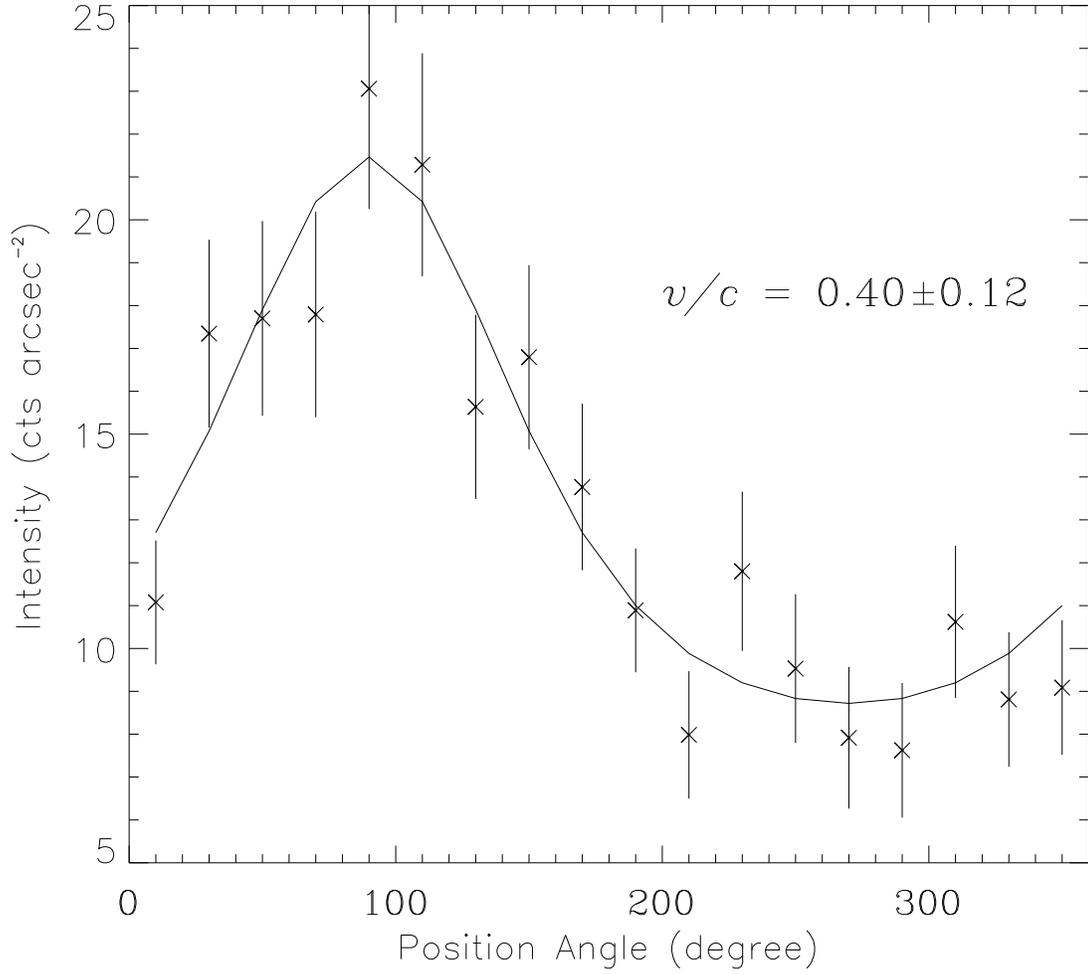
Fig. 5.— The brightness distribution of the X-ray ring vs. position angle (from north to east). Error bars are at 1 σ confidence level. The solid line is the best fit to the data with a Doppler boosting model.